H2NSi radical: structures, isomerisation pathways and electronic states characterization

Majdi Hochlaf, Gilberte Chambaud, Maria Luisa Senent

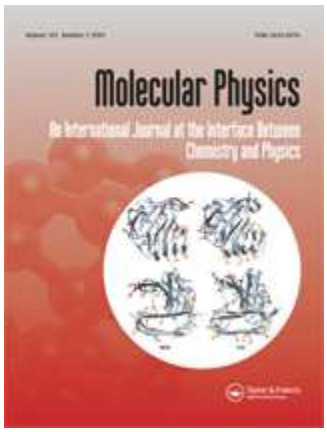

H2NSi radical: structures, isomerisation pathways and electronic states characterization

Journal:	*Molecular Physics*
Manuscript ID:	TMPH-2009-0357.R1
Manuscript Type:	Full Paper
Date Submitted by the Author:	24-Dec-2009
Complete List of Authors:	Hochlaf, Majdi; University of Marne La Vallee, Laboratoire de Chimie Theorique Gilberte, Chambaud; Université de Marne la Vallée Senent, Maria Luisa; IEM-CSIC, DAMIR
Keywords:	ab initio calculations, electronic states, isomers, spectroscopy, silicon compounds
Note: The following files were submitted by the author for peer review, but cannot be converted to PDF. You must view these files (e.g. movies) online.	
New WinZip File.zip	

H_2NSi radical: structures, isomerisation pathways and electronic states characterization*

M. Hochlaf [a)]
Université Paris-Est, Laboratoire de Modélisation et Simulation Multi Echelle, MSME FRE 3160 CNRS, 5 boulevard Descartes, 77454 Marne-la-Vallée, France
E-mail: hochlaf@univ-mlv.fr

G. Chambaud
Université Paris-Est, Laboratoire de Modélisation et Simulation Multi Echelle, MSME FRE 3160 CNRS, 5 boulevard Descartes, 77454 Marne-la-Vallée, France
E-mail: chambaud@univ-mlv.fr

M. L. Senent
Departamento de Astrofísica Molecular e Infrarroja, Instituto de Estructura de la Materia, C.S.I.C., Serrano 121, Madrid 28006, SPAIN
E-mail: senent@iem.cfmac.csic.es

---

a) Author for correspondence.

* dedicated to the memory of Pavel Rosmus.

ABSTRACT

Using state-of-the-art theoretical methods, we investigate the stable isomers of H_2NSi which are relevant for astrophysics, astrochemistry and ammonia silicon surface chemistry. These computations are performed using configuration interaction *ab initio* methods and the aug-cc-pVQZ and cc-pVQZ basis sets. Our calculations confirm the existence of three stable isomers: H_2NSi, *trans*-HSiNH and H_2SiN. We give the intramolecular isomerisation and the H-abstraction reaction pathways on the lowest doublet potential energy surfaces. Insight into the pattern of the lowest doublet and quartet electronic states of these molecular species are also presented.

I. INTRODUCTION

The importance of the silicon-nitrogen bearing compounds is related mainly to the involvement and the role of: (i) silicon atom and ions in the chemistry of the low Earth atmosphere [1-6] and of the ionosphere [7]. (ii) Silicon in astrophysical media either embedded in grains or in gas phase. This domain gained in interest since the detection of SiN in the outer circumstellar envelope IRC +10216 in 1992 by Turner [8] (iii) Silicon atoms and Si^+ ions in gas phase and porous glass surfaces reactivity against ammonia for the production of a wide variety of $Si_xN_yH_z$ molecules and for catalysis [9-11]. (iv) Such molecules in the formation of polysilane materials [12] with, for instance, non linear optics properties. Therefore, $Si_xN_yH_z$ molecules (with small x, y and z numbers), such as H_2NSi radicals of interest here, represent the milestones for this rich and complex chemistry and for its applications.

The H_2NSi^+ positively charged ionic species were widely studied. In a series of papers by Parisel, Hanus and Ellinger [11,13-15], they characterized three stable forms, namely $HSiNH^+$, H_2NSi^+ and H_2SiN^+, using multiconfigurational, Møller-Plesset MPn (n=2,3,4) and Coupled Clusters approaches. They derived the IR and μw spectra of these cations in order to assign the available experimental data and for predictive purposes for astrophysical detections (See Refs. [11,13,15] for more details). In contrast, very few is known on the structure, the isomers, the energetics and the spectroscopy of the H_2NSi neutral tetratomic molecule. This is related to the difficulty to study theoretically open shell molecular systems and to describe correctly their electronic wavefunctions. Moreover, previous works [15] reported: 1) the complexity of the generation of their vibrational spectra. 2) Their floppiness along some internal coordinates (e.g. SiN bond). 3) The difficulty of their isolation in laboratory. 4) Their spontaneous reactivity. Briefly, we can mention the mass spectrometric investigations of Goldberd et al. [16] and of Chen et al. [17], which suggested the formation of HSiNH and H_2NSi either after neutralisation of their respective ions or through reactive collisions between N and SiH_4. These identifications were supported by DFT structure calculations [16-18].

In the present paper, we characterize the stable isomers of H_2NSi by means of state-of-the-art mono and multiconfigurational *ab initio* approaches and extended basis sets. For these species, we derive a set of accurate spectroscopic parameters including their rotational and vibrational terms. Moreover, we study the intramolecular isomerisation and the H-abstraction processes. Finally, we give insight into the pattern of the doublet and the quartet electronic excited states of these tetratomic species in the 0-6 eV internal energy ranges.

II. COMPUTATIONAL DETAILS

Electronic structure calculations have been achieved with the MOLPRO program suite [19]. For these computations, the cc-pVQZ and aug-cc-pVQZ Dunning's basis sets were employed [20,21,22].

We searched for stationary points determining equilibrium geometries and a set of first order spectroscopic parameters (rotational constant, harmonic wavenumbers, dipole moments) at the coupled cluster level including perturbative treatment of triple excitations (RCCSD(T)) [23] and using the standard options in MOLPRO.

We investigated the low lying electronic states of the stable forms of the H_2NSi sum formula with the complete active space self consistent field method (CASSCF) [24,25], followed by internally contracted multi-reference configuration interaction (MRCI) [26,27] approach implemented in MOLPRO [19]. For the CASSCF calculations, all valence molecular orbitals were optimized and all electrons were correlated. For each isomer, the doublets were averaged together and the quartets were averaged together. For MRCI, we took into account all the configurations of the CI expansion of the CASSCF wavefunctions as a reference. For instance, more than 5 x 10^8 uncontracted configuration state functions (CSFs) per C_{2v} symmetry result when computing the doublet states.

Calculations were carried out in the C_1, C_s and C_{2v} point groups. In C_{2v} symmetries, the molecule in lying in the xz plane and the C_2 axis coincides with the z axis allowing the designation of the electronic states. In tables and figures, relative energies are given with respect to that of the most stable isomer ground state equilibrium geometry, except if précised.

III. RESULTS AND DISCUSSION

1. Stable isomers

Figure 1 displays the one-dimensional evolution of HSiNH ground doublet potential energy surface along the torsion coordinate, τ. These calculations were performed with CASSCF, MRCI, MRCI+ Davidson correction (MRCI+Q) [28]) and RCCSD(T). One can clearly see a minimum corresponding to the *trans*-HSiNH (dihedral torsion angle τ = 180°) isomer II (Figure 2). At the CASSCF level, a second local minimum is found for τ=0 (*cis* configuration) and a transition state for τ ~ 80°. Both, the *cis* minimum and the transition state connecting *cis* to *trans* structures, vanish when larger calculations are employed, especially when the dynamical correlation is considered. For the isovalent HCNH molecule, a *cis* form, however, exists and it is located at 4.9 kcal/mol above the *trans* isomer [29]. For that reason, we use RCCSD(T) for the prediction of the structural and spectroscopic properties of the H_2NSi radicals in their ground electronic states.

At the RCCSD(T) level of theory, three stable isomers are found. They are depicted in Figure 2. The most stable form is H_2NSi of C_{2v} symmetry (denoted by isomer I) followed then by *trans*-

HSiNH (isomer II) at ~0.7 eV above and then the H_2SiN of C_{2v} symmetry (isomer III) at ~2 eV (Table 1). These structures are confirmed by MRCI calculations. Our ordering in energy agrees quite well with the MP2/6-31G** calculations of Goldberg et al. [16] and with the recent predictions of Chen et al. [17] obtained with B3LYP/6-311++G(3df,2p). Nevertheless, different assignments are given for the nature of the ground electronic states for the C_{2v} species. Indeed, Goldberg et al. predict a $^2A_1$ space symmetry, whereas Chen et al. found a $^2B_2$ symmetry instead. Our calculations support the results of Chen et al. [17] and the full investigation of the pattern of the lowest electronic states of H_2NSi, HSiNH and H_2SiN (cf. *infra*) confirms these attributions. For the H_2CN isovalent systems, a $^2B_2$ ground state was computed by Puzzarini and Barone for the C_{2v} structures [29].

Table 1 reports the RCCSD(T)/aug-cc-pVQZ equilibrium geometries for the three H_2NSi isomers found presently. For isomer I, our equilibrium geometry is: R_{NH} = 1.010 Å, R_{SiN} = 1.712 Å and the in-plane HNSi angle = 124.2°. For HSiNH, the R_{NH} distance is calculated to be 1.011 Å, the central SiN bond equals to 1.608 Å, R_{HSi} = 1.507 Å, the HSiN angle = 110.6° and the NSiH = 131.9°. For the less stable form (isomer III), we compute: R_{SiH} = 1.488 Å, R_{SiN} = 1.658 Å and HSiN = 126.5°. The optimized geometries with the shorter basis set (cc-pVQZ) are very close to the ones given here.

Table 2 gives the rotational constants of these three isomers at equilibrium (A_e, B_e and C_e) and their dipole moments (μ_e). These radicals present relatively large dipole moments making their identification in astrophysical media feasible by radio spectroscopy. Our work should help for that purpose pursuit in our previous works about silicon molecules of astrophysical interest [30].

Table 2 lists also the harmonic wavenumbers and the infrared intensities for H_2NSi, HSiNH and H_2SiN derived using the standard options of MOLPRO. Calculated intensities for the fundamental bands (see Table 2) can help the assignments of observations through infrared active vibrational modes. For the symmetric modes (a_1, b_2 & a'), the data obtained using the small and the more diffuse basis sets are of the same order of magnitude (differences are less than 50 cm^{-1}), whereas large differences are found for the antisymmetric or for the out-of-plane torsion modes (b_1 & a"). This is most likely because of either the flatness of the potentials along these coordinates or because of numerical problems (symmetry breaking) not fully resolved with the smaller basis set, especially for these floppy molecular systems. Indeed, we showed previously that, for tetratomic weakly bound species, the second order perturbation theory is not fully sufficient for the prediction of their vibrational terms and one needs to go beyond this approximation i.e. to take into account anharmonic effects (more details can be found in Refs. [31-34]). Therefore, the generation of the full 6D potential energy surfaces of the three species of interest here should be performed with the incorporation of diffuse atomic orbitals and multiconfigurational *ab initio* methods and full variational treatment of the nuclear motions.

2. Isomerization pathways

The isomerization process from H_2NSi (I) into *trans*-HSiNH (II) is studied by varying the z_1 distance for different x_1 values. Figure 3 gives the definition of these coordinates. The calculations have been carried out at the CASSCF/MRCI/aug-cc-pVQZ level of theory because of the multiconfigurational nature of the ground doublet wavefunctions along this isomerization pathway. Figure 4 presents the potential curves for the intramolecular isomerization from *trans*-HSiNH (II) into H_2SiN (III) for different z_4 and x_4 values as defined there. For each set of curves, the other internal coordinates are kept fixed at their RCCSD(T)/aug-cc-pVQZ values computed at *trans*-HSiNH ($\tilde{X}\ ^2A'$) equilibrium (Table 1). Our sets of (x_1, z_1) and (x_4, z_4) allow mapping the 6D-PES for H-Si, HSiN and HN and SiNH internal coordinates over wide ranges for the unbroken bonds and the in-plane angles around their equilibrium distances, whereas the lengthened distance (HSi in Figure 3 and HN in Figure 4) varies from -6 up to 10 bohrs. This formally corresponds to relaxation of the internal coordinates.

Figures 3 and 4 show clearly three minima corresponding to the three isomers discussed in previous section. These minima are separated by relatively high potential barriers: E_{I-II} is the isomerization potential barrier energy to convert I into to II and E_{II-III} is the isomerization potential barrier to convert II into III (and *vice versa*). E_{I-II} is estimated to be 2.00 eV and E_{II-III} is calculated to be equal to 3.17 eV. Our MRCI E_{I-II} coincides with the EI-II evaluated at the MP2/6-31G** level [16], whereas our MRCI E_{II-III} value is slightly larger than the MP2 value (2.4 eV) [16], and is believed to be more accurate since they are derived from multiconfigurational treatments and larger basis set than Goldberg et al.'s work [16]. In addition, secondary minima are found which may correspond to transient species of HSiNH (e.g. cf. curve for x_4 = -1.45 & energy ~ 4 eV). This form is located at more than 2 eV relative to the global minimum. More generally, the computed barriers are quite large. Hence, each isomer can *a priori* be isolated for its identification and characterization in laboratory.

In Figures 3 and 4, thick lines correspond to the local potential curves around the minimal structure of each isomer. Each of these curves describes one isomer and not three of them and they don't correspond to the lowest curve at the top of the barrier through these isomerisation pathways. Hence, these processes are accompanied by coordinate relaxation and one needs to consider the 6D-PESs for their dynamical investigations.

The examination of our curves close to the H abstraction channels, producing H + SiNH (channel 1) and H + HSiN (channel 2), reveals that one needs to overcome small potential barriers of ~ 0.15 eV and ~ 0.1 eV before reaching channel 1 products valley from isomers I and II, respectively, whereas the MP2/6-31G** calculations give a direct connection of these tetratomics to their dissociation products. Smaller potential barriers (lower than 0.1 eV) are computed along channel 2 when dissociating isomers II or III. This confirms the MP2/6-31G** previous calculations [16]. Concerning the H-abstraction pathway from isomer I via channel 1, it should occur along the PES of the ground state of this isomer after overcoming the potential barrier of 0.15 eV in addition to the dissociation energy of 1.88 eV (position of H + SiNH asymptote). The production of H + HSiN needs

larger energies (> 4.75 eV) and it goes through the formation of isomer II intermediate and probably also isomer III (Figures 3 and 4). In contrast, our isomer II connects *directly* to channels 1 and 2 products and one needs just to overcome the eventual potential barriers discussed above. For isomer III decomposition, a direct mechanism can be proposed for the formation of H + HSiN whereas the H + HNSi should go through the population of the two other more stable forms.

3. Electronic excited states

Tables 3, 4 and 5 list the dominant electron configuration and the vertical excitation energies of the H_2NSi, HSiNH and H_2SiN doublet and quartet electronic states up to 6 eV. These calculations are performed at the RCCSD(T)/aug-cc-pVQZ equilibrium geometry of their respective ground states (Table 1). These energies are computed using CASSCF and MRCI methodologies and with the cc-pVQZ and aug-cc-pVQZ basis sets. The CASSCF energies of these electronic states are close to those obtained after MRCI treatments. Hence, the static correlation, already included at CASSCF level, is enough for a rather good description. Moreover, the inclusion of diffuse atomic orbitals in the basis set (from cc-pVQZ to aug-cc-pVQZ) does not induce drastic change in the pattern of these electronic states signature of their valence rather than valence-Rydberg nature. Exception should be made for the H_2NSi (3^2A_1) state (Table 3), which is located close to the ionization energy of this molecule [17]. Indeed, its vertical excitation energy is lowered by ~1 eV with the larger basis set.

For H_2NSi and H_2SiN, the first excited states are the 1^2B_1 located at 0.99 eV and 1.37 eV, respectively (Tables 3 and 5). They correspond to the promotion of an electron from the outermost b_1 molecular orbital (MO) to the semi unoccupied b_2 MO. For *trans*-HSiNH, the lowest excited state ($1^2A''$) lies at 2.3 eV with respect to the ground state. Therefore the electronic desexcitation of the HSiNH($1^2A''$) molecules may occur via emission of visible light or radiationless internal conversion processes. For all three isomers, the lowest quartets are located at ~ 3.5 eV above their corresponding ground states.

Strictly speaking, the B_1-B_2 transition (photoemission or absorption) for isomers I and II is forbidden in the C_{2v} point group. Nevertheless, such transition becomes slightly allowed for non symmetrical configurations (C_s or C_1 point groups) i.e. after relaxation of internal coordinates. Accordingly, the unimolecular dynamics of electronically excited H_2NSi and H_2SiN and HSiNH is expected to be very complex.

Generally, a high density of electronic states is found for internal energies > 3 eV. This may favour their mutual interaction by vibronic (at their crossing and avoided crossings) and spin-orbit couplings (at their crossings). In addition, Figure 5, which depicts the one-dimensional evolution of the lowest doublet HSiNH electronic states along the *trans* and *cis* bending coordinates, shows that some of these electronic states correlate to doubly degenerate electronic representations for linear configuration. For instance, this is the case for the second $^2A'$ and the lowest $^2A''$ states which

correlate to the $1^2\Pi$ at linearity. Both components are coupled by Renner-Teller effect. This effect, together with spin-orbit coupling, participates to the mixing of their corresponding wavefunctions especially close to the barriers to linearity. Consequently, generation of the 6D potential energy surfaces of these electronic states and their corresponding rovibronic spectra is computationally challenging. Both the experimental and theoretical spectra are expected to be hard to assign.

IV. CONCLUSION

Using *ab initio* methodologies, we have characterized the stable forms of the astrophysically important H_2NSi radicals, where two C_{2v} structures and a *trans* planar isomer are found. In particular this system does not present a stable *cis* structure in contrast to the isovalent HCNH species. This confirms once more the breakdown of the C/Si analogy which has been point out previously.

For the stable species, we give a set of accurate spectroscopic properties, which are mostly predictive in nature. We explored also their lowest electronic states. These data are useful for the characterization of these species either isolated or trapped in cooled matrices in laboratory by means of μw, IR and UV spectroscopies. This work should motivate their identification in astrophysical media and it should help for the understanding of the gas and condensed phases reactivity of silicon containing molecules and materials with ammonia and small amines.

NOTE

This project has been initiated by discussions with Pavel Rosmus during his last visit to CINECA (Bologna, Italy). We dedicate it to him.

AKCNOWLEGMENTS

The authors acknowledge the *Ministerio de Ciencia e Innovación* of SPAIN for the grants **AYA2008-00446** and **AYA2009-05801-E/AYA** and to CESGA for computing facilities.

REFERENCES

1. D. W. Hughes, in Cosmic Dust, ed. J. A. M. McDonnell, 1978.
2. J. M. C. Plane. Chem. Rev. **103**, 4963 (2003).
3. C. Koeberl and E. H. Hagen. Geochim. Cosmochim. Acta **53**, 937 (1989).
4. T. Vondrak, J. M. C. Plane, S. Broadley and D. Janches. Atmos. Chem. Phys. Discuss. **8**, 14557 (2008).
5. J. C. Gómez Martín, M. A. Blitz and J. M. C. Plane. Phys. Chem. Chem. Phys. **11**, 671 (2009).
6. J. C. Gómez Martín, M. A. Blitz and J. M. C. Plane. Phys. Chem. Chem. Phys. **11**, 671 (2009).
7. E.E. Ferguson, D. W. Fahey, F. C. Fehsenfeld and D. L. Albritton. Planet. Space Sci. **29**, 307, (1981).
8. B. E. Turner. ApJ. **388**, L35 (1992).
9. S. Wlodek and D. K. Bohme. J. Am. Chem. Soc. **110**, 2396 (1988).
10. M. J. D. Low, N. Ramasubramanian and V. V. Subba Rao. J. Phys. Chem. **71**, 1726 (1997).
11. O. Parisel, M. Hanus and Y. Ellinger. Chem. Phys. **212**, 331 (1996).
12. D. Y. Zhang, C. Pouchan, D. Jacquemin and E. A. Perpète. Chem. Phys. Letters **408**, 226 (2005).
13. O. Parisel, M. Hanus and Y. Ellinger. J. Phys. Chem. **100**, 2926 (1996).
14. O. Parisel, M. Hanus and Y. Ellinger. J. Chem. Phys. **104**, 1979 (1996).
15. O. Parisel, M. Hanus and Y. Ellinger. J. Phys. Chem. A **101**, 299 (1999) and references therein.
16. N. Goldberg, J. Hrusak, M. Iraqi and H. Schwarz. J. Phys. Chem. **97**, 10687 (1993).
17. W.-K. Chen, I-Ch. Lu, Ch. Chaudhuri, W.-J. Huang and S.-H. Lee. J. Phys. Chem. A **112**, 8479 (2008).
18. B. S. Jursic. J. Mol. Struct. THEOCHEM **455**, 77 (1998).

19. MOLPRO, A package of ab initio programs, Werner, H.-J., & Knowles, P. J. 2006 (see http://www.molpro.net for more details).

20. T. H. Dunning. J. Chem. Phys. **90**, 1007 (1989).

21. D. E Woon and T. H. Dunning, Jr. J. Chem. Phys. **98**, 1358 (1993).

22. R. A. Kendall, T. H. Dunning, Jr., and R. J. Harrison, J. Chem. Phys. 96,. 6796 1992.

23. P. J. Knowles, C. Hampel and H.-J. Werner. J. Chem. Phys. **99**, 5219 (1993).

24. P.J. Knowles and H.-J. Werner. Chem. Phys. Lett. **115**, 259 (1985).

25. H.-J. Werner and P.J. Knowles. J. Chem. Phys. **82**, 5053 (1985).

26. P.J. Knowles and H.-J. Werner. Chem. Phys. Lett. **145**, 514 (1988).

27. H.-J. Werner and P.J. Knowles. J. Chem. Phys. **89**, 5803 (1988).

28. S.R. Langhoff and E.R. Davidson. Int. J. Quant. Chem. **8**, 61 (1974).

29. C. Puzzarini and V. Barone. Chem. Phys. Letters **467**, 276 (2009) and references therein.

30. N. Inostroza, M. Hochlaf, M. L. Senent and R. Letelier. A & A **486**, 1047 (2008).

31. M. Hochlaf, C. Léonard, E. E. Ferguson, P. Rosmus, E. A. Reinsch, S. Carter and N. C. Handy. J. Chem. Phys. **111**, 4948 (1999).

32. C. Léonard, P. Rosmus, S. Carter and N. C. Handy. J. Phys. Chem. A **103**, 1846 (1999).

33. M. Hochlaf. "Theoretical spectroscopy of tetratomic molecules". Trends in Chemical Physics **12**, 1 (2005).

34. V. Brites, O. Dopfer and M. Hochlaf. J. Phys. Chem. A **112**, 11283 (2008).

Figure captions

Figure 1: One dimensional cut of the 6D potential energy surface of the ground electronic state of *trans*-HSiNH along the torsion (τ) angle.

Figure 2: Stable isomers of H_2SiN and definition of their internal coordinates.

Figure 3: CASSCF/MRCI/aug-cc-pVQZ potential energy curves vs. z_1 for different x_1 values. These curves are given relative to the isomer I minimum. The NH and SiN distances and the in-plane SiNH angle are kept fixed at their RCCSD(T)/aug-VQZ values computed at *trans*-HSiNH ($\tilde{X}\ ^2$A') equilibrium (cf. Table 1).

Figure 4: CASSCF/MRCI/aug-cc-pVQZ potential energy curves vs. z_1 for different x_1 values. These curves are given relative to the isomer I minimum. The SiH and SiN distances and the in-plane HSiN angle are kept fixed at their RCCSD(T)/aug-VQZ values computed at *trans*-HSiNH ($\tilde{X}\ ^2$A') equilibrium (cf. Table 1).

Figure 5: CASSCF/MRCI/aug-cc-pVQZ one dimensional cuts of the 6D potential energy surfaces of the doublet electronic states of HSiNH vs. the *trans* (right side) and *cis* (left side) bending coordinates. The stretchings are kept set to their equilibrium values in *trans*-HSiNH ($\tilde{X}\ ^2$A') (Table 1). The reference energy is the energy of the ground state at linearity.

Photo: Pavel Rosmus (1938-2009).

Table 1: Relative energy (E_R, in eV) and structural parameters (distances in Å; angles in degrees) of H_2NSi isomers. First entry is for the RCCSD(T)/cc-pVQZ data and the second entry is for the RCCSD(T)/aug cc-pVQZ results. See Figure 2 for the definition of the internal coordinates.

Isomer	E_R	R_1	R_2	R_3	θ_1	θ_2	τ
I: $\tilde{X}\,^2B_2$ C_{2v}	0.0 [a]	1.012	1.012	1.711	124.4	124.4	0
		1.010	1.010	1.712	124.2	124.2	0
II: $\tilde{X}\,^2A'$ C_s	0.68	1.509	1.609	1.011	110.3	131.7	180
		1.507	1.608	1.009	110.6	131.9	180
III: $\tilde{X}\,^2B_2$ C_{2v}	1.88	1.488	1.488	1.654	127.0	127.0	0
		1.489	1.489	1.658	126.5	126.5	0

a) Used as reference.

Table 2: Equilibrium rotational constants (A_e, B_e and C_e, in cm^{-1}), harmonic wavenumbers (ω_i, in cm^{-1}) and dipole moment (μ_e, in Debye) of H_2NSi isomers. First entry is for the RCCSD(T)/cc-pVQZ data and the second entry is for the RCCSD(T)/aug cc-pVQZ results. In italic, the IR intensities are defined in $Debyes^2/Å^2amu$.

Isomer	A_e	B_e	C_e	ω_1	ω_2	ω_3	ω_4	ω_5	ω_6	μ_e
H_2NSi (I)	12.0005	0.5113	0.4904	3606.5 (a_1)	1481.9 (a_1)	922.5 (a_1)	838.9 (b_1)	3717.4 (b_2)	884.7 (b_2)	
	11.9936	0.5104	0.4896	3533.3 *20*	1585.0 *7*	729.8 *33*	564.8 *100*	3626.5 *16*	865.1 *3*	2.19
HSiNH (II)	7.4241	0.5879	0.5447	3693.4 (a')	2085.3 (a')	1138.6 (a')	778.2 (a')	445.1 (a')	636.0 (a")	
	7.4773	0.5873	0.5445	3638.3 *25*	2058.3 *100*	1066.9 *8*	726.1 *38*	639.0 *100*	524.0 *40*	1.58
H_2SiN (III)	5.9199	0.5696	0.5196	2210.3 (a_1)	1050.4 (a_1)	959.1 (a_1)	718.5 (b_1)	2232.3 (b_2)	709.2 (b_2)	
	5.8375	0.5681	0.5177	2196.0 *27*	1074.1 *32*	975.3 *29*	509.7 *9*	2195.6 *100*	631.5 *62*	3.37

Table 3: Pattern of the lowest doublet and quartet electronic states of isomer I computed at the RCCSD(T)/aug-cc-pVQZ equilibrium geometry of the ground state. Energies are in eV. We also give their dominant electron configuration.

State	Dominant electron configuration	CASSCF/cc-pVQZ	MRCI/cc-pVQZ	CASSCF/aug-cc-pVQZ	MRCI/aug-cc-pVQZ
$\tilde{X}\ ^2B_2$	$(5a_1)^2(6a_1)^2(2b_2)^2(2b_1)^2\ (7a_1)^2(3b_2)^1$	0.00 [a)]	0.00 [a)]	0.00 [a)]	0.00 [a)]
1^2B_1	$(5a_1)^2(6a_1)^2(2b_2)^2(2b_1)^2\ (7a_1)^2(3b_1)^1$	1.21	1.00	1.17	0.99
1^4A_2	$(5a_1)^2(6a_1)^2(2b_2)^2(2b_1)^2(7a_1)^1(3b_2)^1(3b_1)^1$	3.73	3.56	4.26	3.70
1^2A_1	$(5a_1)^2(6a_1)^2(2b_2)^2(2b_1)^2\ (7a_1)^2(8a_1)^1$	4.08	3.68	2.96	3.18
2^2A_1	$(5a_1)^2(6a_1)^2(2b_2)^2(2b_1)^2\ (7a_1)^1(3b_2)^2$	5.18	4.79	4.84	4.65
1^4B_2	$(5a_1)^2(6a_1)^2(2b_2)^2(2b_1)^1(7a_1)^2(3b_2)^1(3b_1)^1$	4.635	4.95	5.43	5.16
1^2A_2	$(5a_1)^2(6a_1)^2(2b_2)^2(2b_1)^2(7a_1)^1(3b_2)^1(3b_1)^1$	5.56	5.22	5.52	5.20
2^2B_2	$(5a_1)^2(6a_1)^2(2b_2)^2(2b_1)^1(7a_1)^2(3b_2)^1(3b_1)^1$	5.31	5.48	5.39	5.51
2^2B_1	$(5a_1)^2(6a_1)^2(2b_2)^2(2b_1)^1(7a_1)^2(3b_2)^2$	5.32	5.50	5.52	5.55
3^2A_1	$(5a_1)^2(6a_1)^2(2b_2)^2(2b_1)^2(7a_1)^1(3b_1)^2$ & $(5a_1)^2(6a_1)^2(2b_2)^2(2b_1)^2(7a_1)^2(9a_1)^1$	7.16	6.68	6.45	5.58

a) Used as reference.

Table 4: Pattern of the lowest doublet and quartet electronic states of isomer II computed at the RCCSD(T)/aug-cc-pVQZ equilibrium geometry of the ground state. Energies are in eV. We also give their dominant electron configuration.

State	Dominant electron configuration	CASSCF/cc-pVQZ	MRCI/cc-pVQZ	CASSCF/aug-cc-pVQZ	CASSCF/aug-cc-pVQZ
$\tilde{X}\ ^2$A'	$(9a')^2(2a'')^2(10a')^1$	0.00 [a)]	0.00 [a)]	0.00 [a)]	0.00 [a)]
1^2A''	$(9a')^2(2a'')^1(10a')^2$	2.27	2.32	2.22	2.31
2^2A''	$(9a')^2(2a'')^2(3a'')^1$	2.91	2.69	2.94	2.69
2^2A'	$(9a')^1(2a'')^2(10a')^2$	2.98	2.94	2.96	2.93
1^4A'	$(9a')^2(2a'')^1(10a')^1(3a'')^1$	3.58	3.49	3.66	3.49
1^4A''	$(9a')^1(2a'')^2(10a')^1(3a'')^1$	4.32	4.21	4.39	4.20
3^2A'	$(9a')^2(2a'')^1(10a')^1(3a'')^1$	4.88	4.67	4.86	4.65
4^2A'	$(9a')^2(2a'')^2(11a')^1$	5.57	5.30	5.46	5.17
3^2A''	$(9a')^1(2a'')^2(10a')^1(3a'')^1$	5.40	5.40	5.89	5.40

a) Used as reference.

Table 5: Pattern of the lowest doublet and quartet electronic states of isomer III computed at the RCCSD(T)/aug-cc-pVQZ equilibrium geometry of the ground state. Energies are in eV. We also give their dominant electron configuration.

State	Dominant electron configuration	CASSCF/cc-pVQZ	MRCI/cc-pVQZ	CASSCF/cc-pVQZ	MRCI/cc-pVQZ
$\tilde{X}\ ^2B_2$	$(5a_1)^2(6a_1)^2(2b_2)^2(7a_1)^2(2b_1)^2(3b_2)^1$	0.00 [a)]	0.00 [a)]	0.00 [a)]	0.00 [a)]
1^2B_1	$(5a_1)^2(6a_1)^2(2b_2)^2(7a_1)^2(2b_1)^1(3b_2)^2$	1.41	1.36	1.50	1.37
1^2A_1	$(5a_1)^2(6a_1)^2(2b_2)^2(7a_1)^1(2b_1)^2(3b_2)^2$	1.85	1.85	1.84	1.84
1^4B_2	$(5a_1)^2(6a_1)^2(2b_2)^2(7a_1)^2(2b_1)^1(3b_2)^1(3b_1)^1$	3.02	2.90	2.72	2.82
2^2B_2	$(5a_1)^2(6a_1)^2(2b_2)^2(7a_1)^2(2b_1)^1(3b_2)^1(3b_1)^1$	3.90	3.91	3.84	3.88
1^4A_2	$(5a_1)^2(6a_1)^2(2b_2)^2(7a_1)^1(2b_1)^2(3b_2)^1(3b_1)^1$	4.38	4.17	4.09	4.10
2^2B_1	$(5a_1)^2(6a_1)^2(2b_2)^2(7a_1)^2(2b_1)^2(3b_1)^1$	4.30	4.19	4.14	4.15
1^2A_2	$(5a_1)^2(6a_1)^2(2b_2)^2(7a_1)^1(2b_1)^2(3b_2)^1(3b_1)^1$	4.57	4.54	4.37	4.49
1^4A_1	$(5a_1)^2(6a_1)^2(2b_2)^2(7a_1)^1(2b_1)^1(3b_2)^2(3b_1)^1$	4.74	4.63	4.44	4.54
3^2B_2	$(5a_1)^2(6a_1)^2(2b_2)^2(7a_1)^2(2b_1)^1(3b_2)^1(3b_1)^1$ & $(5a_1)^2(6a_1)^2(2b_2)^1(7a_1)^2(2b_1)^2(3b_2)^2$	5.70	5.30	5.56	5.24
2^4A_2	$(5a_1)^2(6a_1)^2(2b_2)^2(7a_1)^2(2b_1)^1(3b_2)^1(8a_1)^1$	6.00	5.60	5.64	5.43
3^2B_1	$(5a_1)^2(6a_1)^2(2b_2)^2(7a_1)^2(3b_2)^2(3b_1)^1$	5.79	5.79	5.79	5.75
2^2A_1	$(5a_1)^2(6a_1)^2(2b_2)^2(7a_1)^1(2b_1)^1(3b_2)^2(3b_1)^1$	5.92	5.89	5.87	5.87

a) Used as reference.

Figure 1

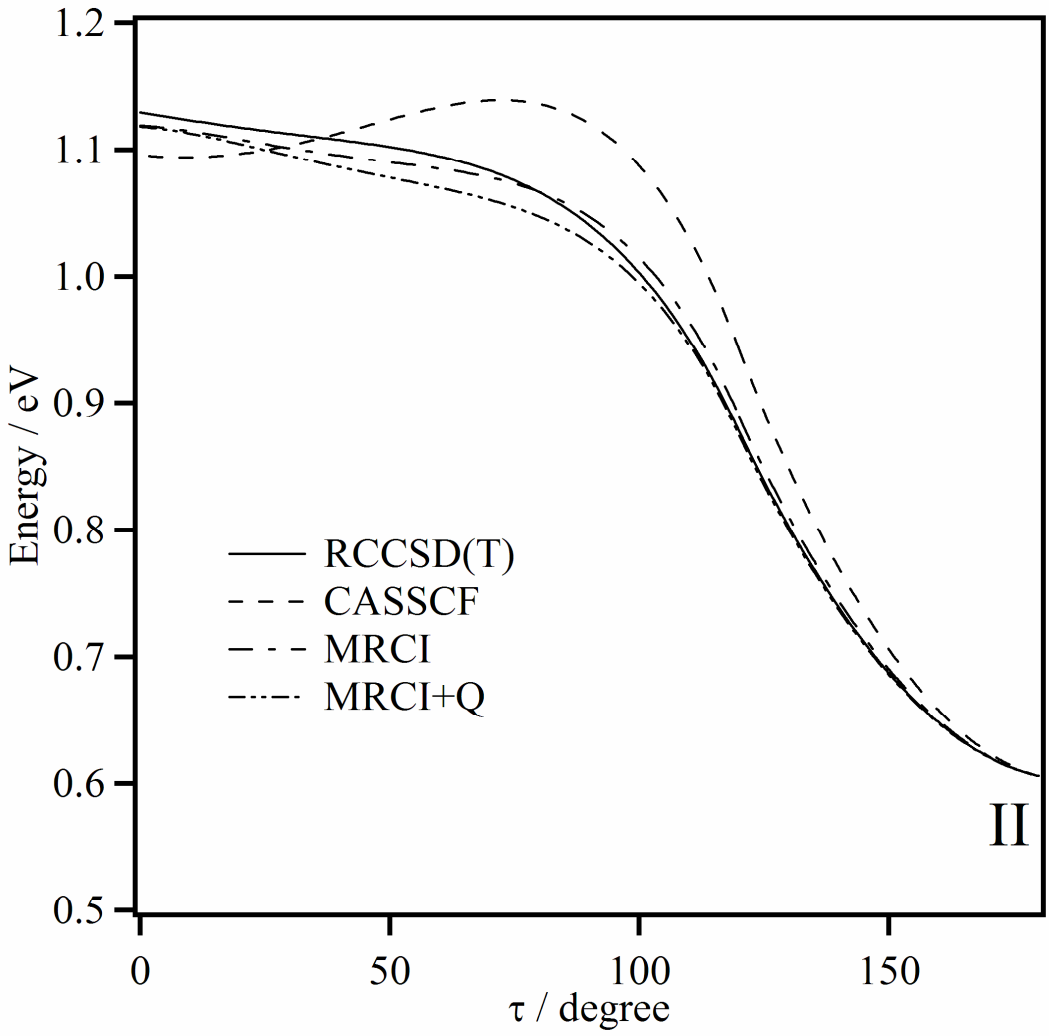

Figure 2

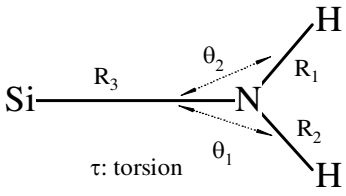

Isomer I

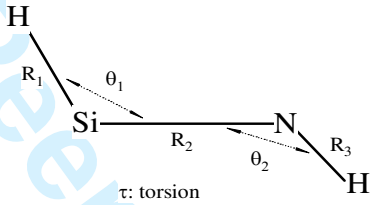

Isomer II

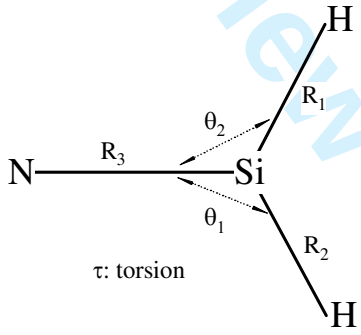

Isomer III

Figure 3

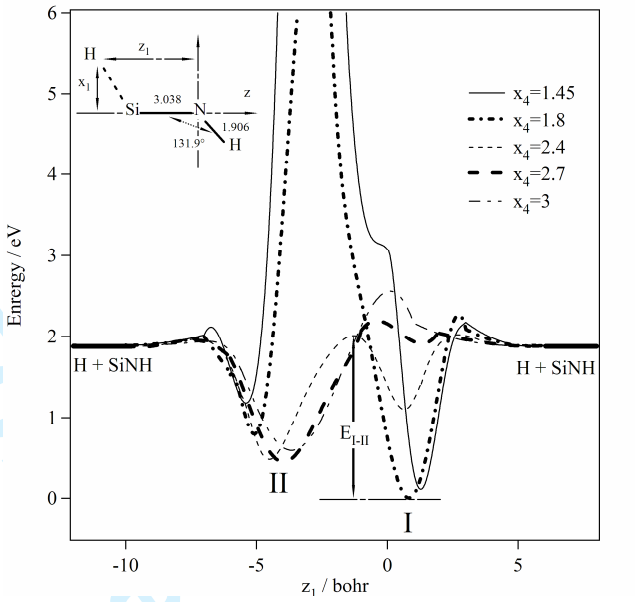

Figure 4

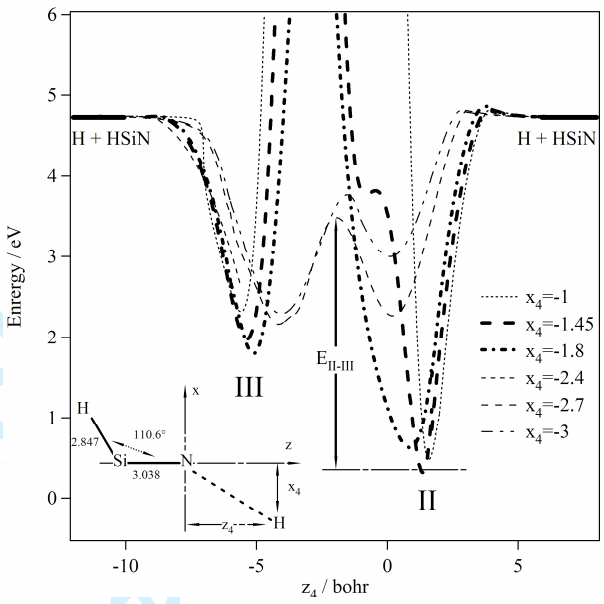

Figure 5

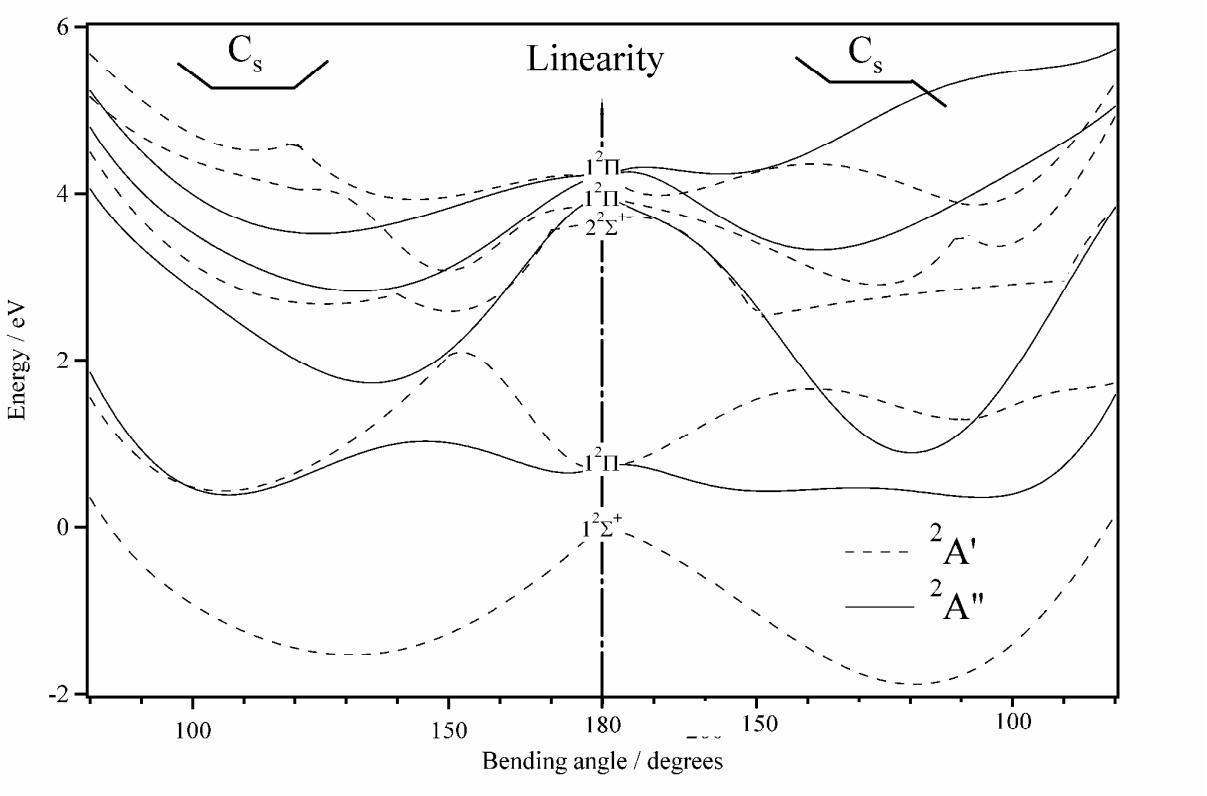

Photo